



Buckling of sandwich beams with compliant interfaces

K. Yu. Volokh ^{a,*}, A. Needleman ^b

^a Faculty of Civil Engineering, Technion—Israel Institute of Technology, Haifa 32000, Israel

^b Division of Engineering, Brown University, Providence, RI 02912, USA

Received 20 September 2001; accepted 20 February 2002

Abstract

Buckling of elastic sandwich beams is analyzed accounting for the compliance of the interfaces between the skin and core. A relation between tractions and displacement jumps across the interfaces characterizes the interfacial compliance. Timoshenko co-rotational beam elements are used to discretize each layer of the sandwich. The dependence of the bifurcation load on the stiffness of the core and on the interfacial compliance are illustrated by considering examples of a sandwich beam with two sets of boundary conditions. It is shown that the load at bifurcation buckling is sensitive to the compliance of the interfaces and that a sufficiently large interfacial compliance can significantly decrease the bifurcation load.

© 2002 Elsevier Science Ltd. All rights reserved.

Keywords: Buckling; Bifurcation; Delamination; Sandwich beams; Non-linear analysis

1. Introduction

Layered structures occur in a wide variety of applications. They are widely used in aircraft, shipbuilding and construction industries because of their favorable strength to weight ratio; they also appear as thin film–substrate systems for electronic packaging applications. Depending on the geometry and loading system, interfacial debonding and structural buckling are possible failure modes. Each of these has been studied extensively. In this paper, we investigate the interaction between these two failure modes.

There is an extensive literature on interfacial debonding of layered solids. Hutchinson and Suo [9] have reviewed results on fracturing of multilayers including delamination of thin films. More recent studies of delamination include those of Gioia and Ortiz [8], Wei and Hutchinson [20] and Choi et al. [4]. An early investigation of the effect of an existing crack on overall stability was carried out by Markstrom and Storakers [15]. More

recently, Frostig and Sokolinsky [6] have analyzed the effect of a pre-existing crack on the buckling of sandwich beams while Sheinman et al. [18] included the growth of delamination into their analysis of the buckling of composite beams.

The focus here is on the interaction between bifurcation buckling and non-zero interfacial compliance, i.e., a delamination has not formed but the interfaces can no longer be regarded as perfectly bonded. The extent to which the non-zero compliance of the interfaces affects the onset of bifurcation buckling is investigated. There have been relatively few investigations of this interaction. Comiez et al. [3] used a beam on the unilateral elastic foundation for modeling the delamination buckling of structures. The latter authors as well as other investigators (e.g. [10]) have considered surface delaminations leading to skin debonding. Bigoni et al. [2] investigated the role of interfacial compliance on the stability of a thin layer bonded to a substrate and Bigoni and Gei [23] bifurcations of a coated elastic cylinder.

In this paper, the effect of interfacial compliance on the buckling of sandwich beams is investigated. Numerical examples are given for a range of values of Young's modulus of the core and of the interfacial compliance to illustrate the role of a sufficiently large

* Corresponding author. Tel.: +972-4-8292413; fax: +972-4-8323433.

E-mail address: cvolokh@aluf.technion.ac.il (K. Yu. Volokh).

interfacial compliance in decreasing bifurcation loads even before delamination takes place.

2. Formulation

The potential energy of an elastic layered structure consisting of r layers and subject to prescribed tractions may be written in the following form:

$$\psi = \sum_{s=1}^r \int_{V_s} W_s dV - \sum_{j=1}^{r-1} \int_{A_j} \phi_j dA - \lambda \int_A \mathbf{T} \cdot \mathbf{u} dA \quad (1)$$

W_s is the strain energy of the s th layer; ϕ_j is the potential of the cohesive surface; $\lambda \mathbf{T}$ are the prescribed surface tractions of magnitude λ ; and \mathbf{u} is the displacement field.

The displacement field is obtained from the equilibrium equations:

$$\delta\psi = \psi_{,\mathbf{u}}(\mathbf{u}, \lambda)[\delta\mathbf{u}] = 0 \quad (2)$$

where brackets designate a linear form.

The structure is stable if the equilibrium state corresponds to a minimum of the potential energy that is attained if

$$\{\psi(\mathbf{u} + \delta\mathbf{u}) - \psi(\mathbf{u})\} / \|\delta\mathbf{u}\|^2 > c > 0 \quad (3)$$

where the displacement variations are kinematically admissible.

The smallest value of λ leading to violation of condition (3) gives the buckling load. In structural applications, (3) is usually equivalent to vanishing of the second variation of the potential energy [12]. After discretization, vanishing of the second variation of the potential energy corresponds to loss of positive definiteness of the Hessian matrix of the discretized potential energy.

In two dimensions, the potential of the cohesive surface is written in the form:

$$\phi = \phi_n + \phi_n \left(1 + \frac{\Delta_n}{\delta_n}\right) \exp\left(-\frac{\Delta_n}{\delta_n} - \frac{\Delta_t^2}{\delta_n^2}\right) \quad (4)$$

where ϕ_n is the work of separation; δ_n is the characteristic length; $\Delta_n = \mathbf{n} \cdot \Delta$ and $\Delta_t = \mathbf{t} \cdot \Delta$ with \mathbf{n} and \mathbf{t} as the normal and tangent, respectively, to the surface at the given point in the reference configuration. The form of ϕ in (4) is a special case of the type of potentials given in [19].

Differentiating the cohesive surface potential, one derives the normal and tangent tractions that are conjugate to the displacement jumps across the cohesive surface

$$T_n = \frac{\partial\phi}{\partial\Delta_n} = -\frac{\phi_n \Delta_n}{\delta_n^2} \exp\left(-\frac{\Delta_n}{\delta_n} - \frac{\Delta_t^2}{\delta_n^2}\right) \quad (5)$$

$$T_t = \frac{\partial\phi}{\partial\Delta_t} = -2\frac{\phi_n \Delta_t}{\delta_n^2} \left(1 + \frac{\Delta_n}{\delta_n}\right) \exp\left(-\frac{\Delta_n}{\delta_n} - \frac{\Delta_t^2}{\delta_n^2}\right) \quad (6)$$

From (5) and (6) it can be seen that the magnitude of the normal and tangential stiffnesses at $\Delta_n = \Delta_t = 0$ are ϕ_n/δ_n^2 and $2\phi_n/\delta_n^2$ respectively.

Each layer is considered as Timoshenko (Reissner–Mindlin) beam, which is appropriate when the half-length of the deformation wave is not less than the layer thickness, and the strain energy takes the form:

$$W = 0.5EA \int \varepsilon^2 dx + 0.5EI \int \chi^2 dx + 0.5GA \int \gamma^2 dx \quad (7)$$

where EI , EA , GA are the bending, axial, and shear stiffness. For small strains and large rotations the strain measures may be written in the form:

$$\varepsilon = \frac{du}{dx} + \frac{1}{2} \left(\frac{du}{dx}\right)^2 + \frac{1}{2} \left(\frac{dw}{dx}\right)^2; \quad \chi = -\frac{d\theta}{dx}; \quad \gamma = -\theta + \arcsin \frac{dw}{dx} \quad (8)$$

where u is an axial displacement; w is a transverse displacement; and θ is the rotation of the normal. The non-linear terms in the strain–displacement relations allow excluding large rotations and translations. Thus small strains are superposed on rigid body motions. The latter approach is known as “co-rotational” [1,5]. Accounting for geometrical non-linearity is crucial for performing a non-linear buckling analysis.

3. Finite element implementation

The aforementioned assumptions lead to the following discrete total energy for the sandwich beam shown in Fig. 1:

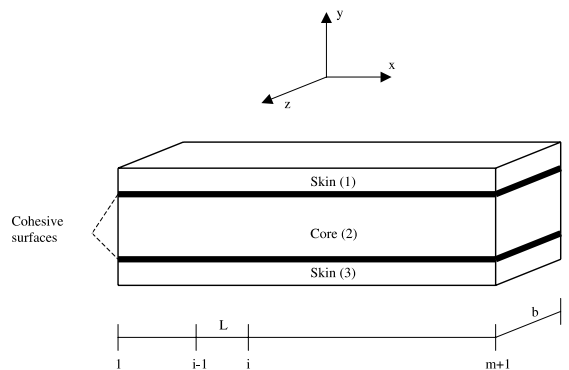


Fig. 1. A sandwich beam.

$$\begin{aligned} \psi(\mathbf{v}, \lambda) = & \frac{L}{2} \sum_{s=1}^3 \sum_{i=1}^m \{ (EI)_s \chi_{si}^2 + (GA)_s \gamma_{si}^2 + (EA)_s \varepsilon_{si}^2 \} \\ & - Lb\phi_n \sum_{j=1}^2 \sum_{i=1}^m \left\{ 1 + \frac{A_{nji} + A_{n\bar{j}i+1}}{2\delta_n} \right\} \\ & \times \exp \left\{ -\frac{A_{n\bar{j}i} + A_{n\bar{j}i+1}}{2\delta_n} - \left(\frac{A_{lji} + A_{l\bar{j}i+1}}{2\delta_n} \right)^2 \right\} \\ & - \lambda f(\mathbf{T})[\mathbf{u}] \end{aligned} \quad (9)$$

where

$$\begin{cases} \Delta_{n1i} = w_{1i} - w_{2i} \\ \Delta_{n2i} = w_{2i} - w_{3i} \\ \Delta_{l1i} = (u_{1i} + h_1\theta_{1i}/2) - (u_{2i} - h_2\theta_{2i}/2) \\ \Delta_{l2i} = (u_{2i} + h_2\theta_{2i}/2) - (u_{3i} - h_3\theta_{3i}/2) \end{cases} \quad (10)$$

$$\begin{cases} \chi_{si} = (\theta_{si} - \theta_{si+1})/L \\ \gamma_{si} = \alpha_{si} - (\theta_{si} + \theta_{si+1})/2 \\ \varepsilon_{si} = \eta_{si}/L \end{cases} \quad (11)$$

$$\begin{cases} \alpha_{si} = \arcsin((w_{si+1} - w_{si})/(L + \eta_{si})) \\ \eta_{si} = (u_{si+1} - u_{si}) + (1/2L)(u_{si+1} - u_{si})^2 \\ \quad + (1/2L)(w_{si+1} - w_{si})^2 \\ L = L_b/m \end{cases} \quad (12)$$

Here, all element lengths are of equal length (L) along the beam for every layer; $(EI)_s$, $(EA)_s$, $(GA)_s$ are the bending, axial, and shear stiffness of the s th layer, respectively; u_{si} , w_{si} are axial and lateral displacements of the i th nodal point of the middle plane of the s th layer; θ_{si} is the i th cross-sectional rotation of the s th layer; α_{si} is a rigid body rotation of the i th element of the s th layer; h_s is the s th layer height; b is the beam width; \mathbf{u} is a vector of generalized nodal displacements including u_{si} , w_{si} , θ_{si} ; and f is the discrete load potential, which is a linear form with respect to \mathbf{u} .

By imposing kinematic and traction boundary conditions, the problem is specified as described subsequently. Arc-length type procedures are used to trace the equilibrium path of the structure for the prescribed load. In order to follow the equilibrium path of the structure in its state space it is useful to introduce the column matrix of the unbalanced nodal forces and the tangent stiffness matrix

$$\mathbf{g} = \frac{\partial \psi}{\partial \mathbf{u}} = \mathbf{B}^T \mathbf{p} - \lambda \mathbf{q} = 0 \quad (13)$$

$$\mathbf{K} = \frac{\partial \mathbf{g}}{\partial \mathbf{u}}; \quad \mathbf{q} = -\frac{\partial \mathbf{g}}{\partial \lambda} \quad (14)$$

It is assumed that the external load gives rise to fixed \mathbf{q} but its magnitude is proportional to the parameter λ . A variety of approaches exist for solving Eq. (13): [5,7, 11,13,14,16,17,21].

The basic procedure for tracing a monotonically changing equilibrium path is the Newton–Raphson algorithm:

Box 1

1. Input: a point on the equilibrium path ($\mathbf{u}, \lambda, \mathbf{g}, \mathbf{K}$).
2. Load increment: $\lambda \leftarrow \lambda + d\lambda$ and updating \mathbf{g} .
3. Computation: $d\mathbf{u} = -\mathbf{K}^{-1}\mathbf{g}$.
4. Updating: $\mathbf{u} \leftarrow \mathbf{u} + d\mathbf{u}$ and \mathbf{g}, \mathbf{K} .
5. Go to step 2 if the convergence criterion is satisfied or return to step 3 otherwise.

This algorithm is unable to treat points where the equilibrium path does not exist for increasing parameter λ or branching occurs. Arc-length continuation is better suited to these situations:

Box 2

1. Input: a point on the equilibrium path ($\mathbf{u}, \lambda, \mathbf{g}, \mathbf{K}$).
2. Arc-length increment: ds .
3. Predictor (initial guess): $\mathbf{y} = \mathbf{K}^{-1}\mathbf{q}; d\lambda = ds/\sqrt{\mathbf{y}^T\mathbf{y} + 1}; d\mathbf{u} = d\lambda\mathbf{y}$.
4. Updating: $\mathbf{u} \leftarrow \mathbf{u} + d\mathbf{u}; \lambda \leftarrow \lambda + d\lambda; \mathbf{g}, \mathbf{K}$.
5. Corrector: $d\mathbf{v} = \mathbf{K}^{-1}\mathbf{q}; d\mathbf{w} = \mathbf{K}^{-1}\mathbf{g}; \delta\lambda = -(\mathbf{du}^T d\mathbf{w})/(\mathbf{du}^T d\mathbf{v}); d\mathbf{u} = d\mathbf{w} + \delta\lambda d\mathbf{v}$.
6. Updating: $d\mathbf{u} \leftarrow d\mathbf{u} + d\mathbf{u}; \mathbf{u} \leftarrow \mathbf{u} + d\mathbf{u}; d\lambda \leftarrow d\lambda + \delta\lambda; \lambda \leftarrow \lambda + \delta\lambda; \mathbf{g}, \mathbf{K}$.
7. Go to step 2 if the convergence criterion is satisfied or return to step 5 otherwise.

It may be seen from Box 2, that the arc-length parameter ds controls the advance along the equilibrium path and that any turning point is readily treated. In contrast to the Newton–Raphson procedure (Box 1) the first and subsequent iterations are distinguished and called predictor and corrector steps accordingly. A wide variety of predictors and correctors have been proposed in the literature: [5,17]. It is possible, for example, to find the corrector by applying the Newton–Raphson procedure to some augmented system of non-linear equations, which include Eq. (13) together with some arc-length constraint. Such an approach is called ‘consistent’ by some authors [21]. In this sense, the algorithm given in Box 2 is ‘inconsistent’. However, it was found to be efficient in the present computations.

The arc-length continuation algorithm needs to be slightly modified to allow for branch switching. Particularly, the predictor guess \mathbf{y} should be close to the branch emanating from the bifurcation point while $d\lambda$ can be set zero. There are two main strategies to define \mathbf{y} . The first one is to pinpoint the equilibrium point and then to find \mathbf{y} as the singular vector of \mathbf{K} at this point.

The main drawback of this strategy is the necessity of dealing with an ill conditioned matrix \mathbf{K} as the bifurcation point is approached. The second strategy is to define \mathbf{y} as the eigenvector corresponding to the smallest eigenvalue of \mathbf{K} without pinpointing the bifurcation point. In any case, the scaling parameter for \mathbf{y} needs to be fit by a trial and error procedure.

Points where two equilibrium branches intersect are identified by the one-dimensional null space of the tangent stiffness matrix and may be classified as follows:

Box 3

Limit (turning) point: $B_1 \neq 0, B_4 \neq 0$.
 Asymmetric (trans-critical) bifurcation:
 $B_1 \neq 0, B_4 = 0, B_2^2 - B_1 B_3 > 0$.
 Symmetric (pitchfork) bifurcation:
 $B_1 = 0, B_2 \neq 0, B_4 = 0$.
 $B_1 = \frac{d}{d\varepsilon} \Big|_{\varepsilon \rightarrow 0} (\mathbf{z}_1^T \mathbf{K}_1 \mathbf{z}_1)$; $B_2 = \frac{d}{d\varepsilon} \Big|_{\varepsilon \rightarrow 0} (\mathbf{z}_1^T \mathbf{K}_1 \mathbf{z}_2)$;
 $B_3 = \frac{d}{d\varepsilon} \Big|_{\varepsilon \rightarrow 0} (\mathbf{z}_1^T \mathbf{K}_2 \mathbf{z}_2)$; $B_4 = -\mathbf{q}^T \mathbf{z}_1$, $\mathbf{K}_1 = \mathbf{K}(\mathbf{u}^* + \varepsilon \mathbf{z}_1)$;
 $\mathbf{K}_2 = \mathbf{K}(\mathbf{u}^* + \varepsilon \mathbf{z}_2)$; \mathbf{u}^* is a vector of generalized nodal displacements at the bifurcation point;
 $\mathbf{z}_1 = \text{Nullspace } \mathbf{K}^*$, $\|\mathbf{z}_1\| = 1$; $\mathbf{K}^* = \mathbf{K}(\mathbf{u}^*)$;
 $\mathbf{z}_2 = \bar{\mathbf{K}}^{-1} \mathbf{q}$, $\|\mathbf{z}_2\| = 1$; $\bar{\mathbf{K}} = \mathbf{K}^* + \alpha \mathbf{z}_1 \mathbf{z}_1^T$; α is an arbitrary number.

The analysis of the bifurcation point given in Box 3 requires gradients of the tangent stiffness matrix which can be obtained numerically by using approximate techniques or by direct numeric/symbolic computations as available in modern packages such as Maple, Mathematica, Matlab, etc. Knowledge of the type of the bifurcation point is useful for branch switching and further stability analysis, with the stability of the equilibrium path defined by positive definiteness of the tangent stiffness matrix \mathbf{K} .

4. Results

Two sets of boundary conditions for the compressed sandwich beam are considered (Fig. 2a and b). In both cases, the beam is of length L_b ($0 \leq x \leq L_b$) and consists of three layers. The first case is a clamped-free beam (Fig. 2a) with the following constraints imposed on the clamped edge $x = 0$:

$$u_{s1} = w_{s1} = \theta_{s1} = 0, \quad s = 1, 2, 3 \tag{15}$$

The load

$$\lambda f(\mathbf{T})[\mathbf{u}] = -\lambda u_{2m+1} \tag{16}$$

is applied through the stiff vertical plate attached to the face of the beam at $x = L_b$. The vertical plate is modeled by the conditions:

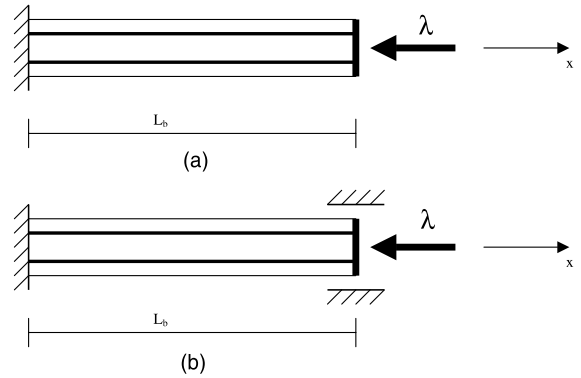


Fig. 2. (a) The clamped-free boundary conditions. (b) The clamped-clamped boundary conditions.

$$\begin{aligned} \Delta_{n1m+1} &= \Delta_{n2m+1} = 0 \\ \Delta_{t1m+1} &= \Delta_{t2m+1} = 0 \\ \theta_{1m+1} &= \theta_{2m+1} = \theta_{3m+1} \end{aligned} \tag{17}$$

The second case is a clamped-clamped beam as shown in Fig. 2b. The boundary conditions at $x = 0, L_b$ are:

$$\begin{aligned} u_{s1} = w_{s1} = \theta_{s1} = w_{sm+1} = \theta_{sm+1} = 0, \quad s = 1, 2, 3 \\ u_{1m+1} = u_{1m+2} = u_{1m+3} \end{aligned} \tag{18}$$

The geometrical parameters of the beam are: $L_b = 0.4m$, $b = 0.02m$, $h_1 = h_3 = 0.001m$, $h_2 = 0.006m$. All layers are isotropic with Poisson’s ratio $\nu = 0.3$; Young’s modulus has the fixed value $E_1 = E_3 = 200 \text{ GPa}$ for the skin layers and various values are used for the core modulus E_2 . The two cohesive surfaces are identical and $\delta_n = 4 \times 10^{-7}m$. The work of separation ϕ_n is assigned various values. Note that from (5) and (6) that the interfacial stiffness scales with ϕ_n .

Results for the computation of the critical bifurcation load for the two sets of boundary conditions considered are presented in Figs. 3 and 4 respectively. In the prebifurcation solution for both loading cases $\Delta_{n1i} = \Delta_{n2i} = \Delta_{t1i} = \Delta_{t2i} = 0$. The parameters varied are Young’s modulus of the core E_2 and the interfacial stiffness through the work of separation ϕ_n . The results presented were obtained for a 60-element mesh ($m = 20$). A finer mesh of 120 elements ($m = 40$) was used as well, which gave bifurcation loads slightly lower in absolute value. The difference, however, did not exceed 2%.

The results show that compliant interfaces can lead to a drastic reduction of the bifurcation load. Considering the examples in Figs. 3 and 4, values of the work of separation larger than $\phi_n = 10^{-1} \text{ J/m}^2$ give nearly the same response as perfect bonding up to the onset of bifurcation for both sets of boundary conditions. If the interface is more compliant, that is if $\phi_n < 10^{-1} \text{ J/m}^2$, then the reduction in the bifurcation load depends on the boundary conditions. The clamped-free boundary conditions provide a longer wavelength of deformation

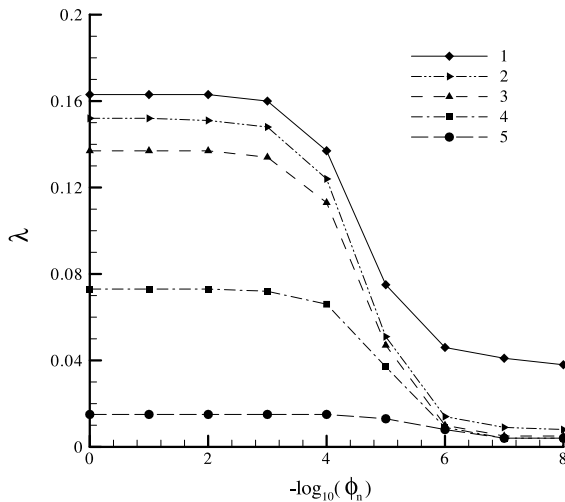


Fig. 3. Bifurcation loads for the clamped-free boundary conditions shown in Fig. 2(a) as a function of ϕ_n which provides a measure of the interfacial compliance for various ratios of the elastic moduli of the skins and the core. The bifurcation load is normalized by a reference load of 10 KN and the value of ϕ_n is normalized by the reference value 1 J/m²: (1) $E_2/E_1 = 10^{-1}$; (2) $E_2/E_1 = 10^{-2}$; (3) $E_2/E_1 = 10^{-3}$; (4) $E_2/E_1 = 10^{-4}$; (5) $E_2/E_1 = 10^{-5}$.

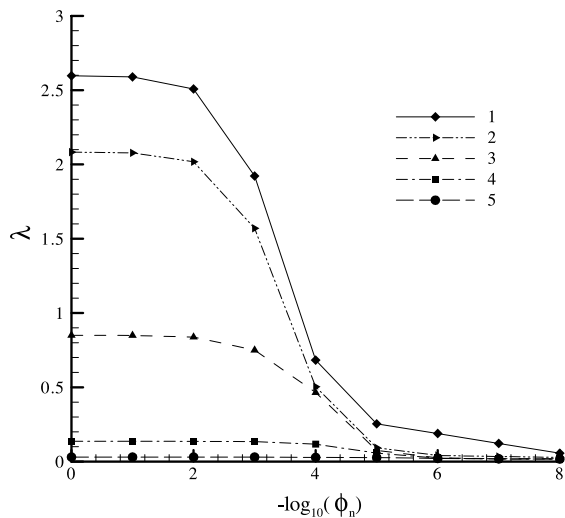


Fig. 4. Bifurcation loads for the clamped-clamped boundary conditions shown in Fig. 2(b) as a function of ϕ_n which provides a measure of the interfacial compliance for various ratios of the elastic moduli of the skins and the core. The bifurcation load is normalized by a reference load of 10 KN and the value of ϕ_n is normalized by the reference value 1 J/m²: (1) $E_2/E_1 = 10^{-1}$; (2) $E_2/E_1 = 10^{-2}$; (3) $E_2/E_1 = 10^{-3}$; (4) $E_2/E_1 = 10^{-4}$; (5) $E_2/E_1 = 10^{-5}$.

while the clamped-clamped boundary conditions provide a shorter one. A slight reduction of the bifurcation

load begins at $\phi_n = 10^{-2}$ J/m² in Fig. 3 for the clamped-free boundary conditions and at $\phi_n = 10^{-1}$ J/m² in Fig. 4 for the clamped-clamped boundary conditions. A significant reduction of the bifurcation load begins when $\phi_n = 10^{-3}$ J/m² in Fig. 3 for the clamped-free boundary conditions and when $\phi_n = 10^{-2}$ J/m² in Fig. 4 for the clamped-clamped boundary conditions. Thus, the more constrained boundary conditions which have a shorter wavelength bifurcation mode are more sensitive to the increase in interfacial compliance.

It is emphasized that, although the non-linear cohesive surface potential was used in the calculations, the equilibrium path is essentially linear up to the bifurcation load.

Results of the analysis of the bifurcation point including the character of the initial postbifurcation behavior are presented in Table 1. Increasing interface compliance reduces the bifurcation load and the postbifurcation modes are bending modes which involve no debonding in the initial postbifurcation regime.

5. Concluding remarks

Numerical simulations of the mechanical response of elastic compressed sandwich beams have been carried out where the beams are three-layer assemblies of geometrically non-linear Timoshenko beam elements. Attention was focused on circumstances where small strains are superposed on possibly large rigid body translations and rotations and the interfaces between layers are taken to be compliant cohesive surfaces. The numerical procedures used for analyzing the response of the compressed sandwich beams include equilibrium path tracing, branch switching, and the analysis of simple critical points. Two sets of boundary conditions, clamped-free and clamped-clamped, were considered for a range of material parameters characterizing the central layer and the interfaces.

The results of numerical calculations show that the first bifurcation load is sensitive to the interface compliance and may significantly decrease for more compliant interfaces. This decrease is especially significant for the clamped-clamped boundary conditions. At least in the circumstances analyzed here, more constrained beams that give rise to a shorter wavelength bifurcation mode and that potentially possess higher load carrying capacity are more susceptible to the adverse effects of having a compliant interface. It is worth emphasizing that the value of the compliance is a property of the interface and not necessarily a property of the physical glue. For example, the glue may be very stiff, but the interface between the glue and the bulk material may be weak and this is what would then set the interfacial compliance.

Table 1

Bifurcation and postbifurcation behavior of the clamped–clamped sandwich beam. The bifurcation loads are normalized by the value for $\phi_n = \infty$ which is denoted by λ_0 and is equal to 25.9 KN ($E_1 = E_3 = 200$ GPa; $E_2 = 20$ GPa; $m = 20$)

ϕ_n (J/m ²)	∞	10^{-2}	10^{-4}	10^{-6}	0
Bifurcation load, λ/λ_0	1	0.965	0.264	0.0730	0.0840
Type of bifurcation point	Unstable simple pitchfork	Unstable simple pitchfork	Unstable simple pitchfork	Unstable simple pitchfork	Compound
Initial postbifurcation mode	Bending	Bending; no delamination	Bending; no delamination	Bending; no delamination	Bending

The interface must be sufficiently compliant; stiff interfaces do not significantly affect the bifurcation load (see Figs. 3 and 4). Since in the bifurcation analyzes here, cohesive surface non-linearity has little effect, Eqs. (5) and (6) can be approximated as

$$T_n = -\frac{\phi_n}{\delta_n^2} A_n, \quad T_t = -2\frac{\phi_n}{\delta_n^2} A_t$$

The quantity $S = \phi_n/\delta_n^2$ characterizes the stiffness of the interface. Although the calculations in Figs. 3 and 4 were carried out for one value of δ_n other calculations not reported here show that over a wide range the bifurcation load depends only on the ratio ϕ_n/δ_n^2 and not on ϕ_n and δ_n separately. Hence, for example, if $\delta_n = 4 \times 10^{-6}m$ the values of ϕ_n in Figs. 3 and 4 at which a significant reduction of the bifurcation load occurs would be increased by two orders of magnitude. The value of the work of separation ϕ_n is directly related to the fracture toughness [24] but as yet there is no standard procedure for obtaining a value of δ_n for specific interfaces. However, experimental means of identifying cohesive parameters are being developed [25]. In any case, the present results indicate that there are values of interfacial stiffness (which depend on the structure) below which bifurcation buckling loads are much reduced.

The first critical point was found to be a simple unstable pitchfork bifurcation with the bifurcation mode being one of pure bending as noted in Table 1. Bifurcation occurs for perfect structures. When the initial postbifurcation behavior is unstable and when inevitable small imperfections are accounted for, limit points are reached with the maximum load set by the magnitude of the imperfection and the character of the bifurcation point, as shown by Koiter's general theory of elastic stability [22].

In the circumstances analyzed here, the effect of increasing interfacial compliance is to reduce the overall structural stiffness and thus precipitate buckling. Hence, interfacial properties can play a significant role in setting the load carrying capacity of a structure even when debonding and the subsequent propagation of a delamination crack have not taken place.

Acknowledgements

The work of K.Y.V. was supported by the Fund for the Promotion of Research at the Technion.

References

- [1] Belytschko T, Liu WK, Moran B. Nonlinear Finite Elements for Continua and Structures. New York: Wiley; 2000.
- [2] Bigoni D, Ortiz M, Needleman A. Effect of interfacial compliance on bifurcation of a layer bonded to a substrate. *Int J Solids Struct* 1997;34:4305–26.
- [3] Comiez JM, Waas AM, Shahavan KW. Delamination buckling; experiment and analysis. *Int J Solids Struct* 1995;32:767–82.
- [4] Choi SR, Hutchinson JW, Evans AG. Delamination of multilayer thermal barrier coatings. *Mech Mater* 1999;31: 431–47.
- [5] Crisfield MA. Nonlinear Analysis of Solids and Structures, vols. 1 and 2. Chichester: Wiley; 1991, 1997.
- [6] Frostig Y, Sokolinsky V. High-order buckling of debonded (delaminated) sandwich panels with a “soft” core. *AIAA J* 2000;38:2147–59.
- [7] Fujii F, Okazawa S. Pinpointing bifurcation points and branch switching. *J Engng Mech* 1997;123:179–89.
- [8] Gioia G, Ortiz M. Delamination of compressed thin films. *Adv Appl Mech* 1997;33:120–93.
- [9] Hutchinson JW, Suo Z. Mixed mode cracking in layered materials. *Adv Appl Mech* 1992;29:64–192.
- [10] Kachanov LM. Delamination Buckling of Composite Materials. Dordrecht: Kluwer; 1988.
- [11] Keller HB. Numerical Methods for Two-Point Boundary-Value Problems. NY: Dover; 1992.
- [12] Koiter WT. A basic open problem in the theory of elastic stability. In: Proceedings of the IUTAM/IMU Symposium On Application of Methods of Functional Analysis to Problems of Mechanics, Marseilles, France. 1975.
- [13] Kouhia R, Mikkola M. Tracing the equilibrium path beyond simple critical points. *Int J Numer Meth Engng* 1989;28:2923–41.
- [14] Magnusson A, Svensson I. Numerical treatment of complete load–deflection curves. *Int J Numer Meth Engng* 1998;41:955–71.
- [15] Markstrom K, Storakers B. Buckling of cracked members under tension. *Int J of Solids Struct* 1980;16:217–21.

- [16] Riks E. Buckling analysis of elastic structures: a computational approach. *Adv Appl Mech* 1998;34:1–76.
- [17] Seydel R. Practical bifurcation and stability analysis: from equilibrium to chaos. second ed. New York: Springer; 1994.
- [18] Sheinman I, Kardomateas GA, Pelegri AA. Delamination growth during pre- and post-buckling phases of delaminated composite laminates. *Int J Solids Struct* 1998;35:19–31.
- [19] Xu XP, Needleman A. Void nucleation by inclusion debonding in a crystal matrix. *Model Simulat Mater Sci Engng* 1993;1:111–32.
- [20] Wei Y, Hutchinson JW. Nonlinear delamination mechanics for thin films. *J Mech Phys Solids* 1997;45:1137–59.
- [21] Wriggers P. Solution strategies for nonlinear equations and computation of singular points. In: Kounadis AN, Kratzig WB, editors. *Nonlinear Stability of Structures: Theory and Computational Techniques*. New York: Springer; 1995.
- [22] Koiter WT. Over de stabiliteit van het elastisch evenwicht. Thesis, Delft, H.J. Paris, Amsterdam, 1945, English translations (a) NASA TT-F10, 1967; (b) AFFDL-TR-70-25, 1970.
- [23] Bigoni D, Gei M. Bifurcations of a coated, elastic cylinder. *Int J Solids Struct* 2001;38:5117–48.
- [24] Rice JR. A path independent integral and the approximate analysis of strain concentration by notches and cracks. *J Appl Mech* 1968;35:379–86.
- [25] Mohammed I, Liechti KM. Cohesive zone modeling of crack nucleation at bimaterial corners. *J Mech Phys Solids* 2000;48:735–64.